

Perturbative QCD at High Energy Colliders¹

Richard J. Gonsalves²

Department of Physics

*University at Buffalo, The State University of New York
Buffalo, NY 14260-1500, USA*

Abstract

Selected applications of perturbative Quantumchromodynamics (QCD) to predictions of the Standard Model for processes at high energy colliders are reviewed with emphasis on past successes and future problems. This is a personal retrospective is not intended to be a comprehensive review of the field.

1 Introduction

It is with great pleasure that I dedicate this contribution to Professor Piyare Lal Jain, a pioneering faculty member in experimental high energy and heavy ion physics at the University at Buffalo over the past fifty years, and a respected senior colleague of mine in the Department of Physics over the past twenty-five years. His mentoring, friendship and collaboration[1] have been invaluable to me.

2 Renormalization Prescription Dependence of QCD Predictions

My earliest work in the field of perturbative QCD with Celmaster[2, 3] was on the renormalization prescription of the effective coupling α_s and its experimental consequences.

Quantumchromodynamics (QCD) is an asymptotically-free quantum field theory. The scaling behavior of Green's functions in the deep Euclidean region can be computed as a perturbation series in the renormalized coupling constant α_s , which depends on the characteristic energy scale involved in the process. This property of QCD was first used to obtain predictions for scale breaking of the naive parton model in deeply-inelastic lepton-hadron scattering. The domain of applicability of perturbative QCD has since been extended to include e^+e^- annihilation to hadrons and numerous other infrared safe observables at high energy colliders[4].

A typical prediction of perturbative QCD is an n -th moment of a structure function in deeply-inelastic scattering[5]

$$M_n = g^{a_n} [1 + b_n g^2 + \mathcal{O}(g^4)] A_n , \quad (1)$$

where $g = \sqrt{4\pi\alpha_s}$ is the $SU(3)_c$ coupling parameter, a_n and b_n are calculable numbers, and the normalization A_n cannot be calculated in perturbation theory. The coefficient b_n depends on how ultraviolet divergences are renormalized, and so implicitly does the coupling g . The renormalization-prescription dependence of b_n must be related to that of g because physical observables cannot depend on how the theory is renormalized. To exhibit this dependence, express g in terms of the coupling g' in a different renormalization scheme:

$$g = g' [1 + a g'^2 + \mathcal{O}(g'^4)] , \quad (2)$$

¹ Contribution to the Symposium: 50+ Years of High Energy Physics at UB, University at Buffalo, October 20-21, 2006. Published in Int. J. Mod. Phys. E **17** (2008) 870-890.

²Email: phygons@buffalo.edu

where a is a calculable constant. To obtain the coefficient b'_n in the second scheme, substitute the expression for g in Eq. (2) in Eq. (1):

$$M_n = (g')^{a_n} [1 + (b_n + aa_n)g'^2 + \mathcal{O}(g'^4)] A_n = (g')^{a_n} [1 + b'_n g'^2 + \mathcal{O}(g'^4)] A_n . \quad (3)$$

If the perturbation series in Eqs. (1,3) were known to all orders in the couplings g, g' , then the renormalization-prescription dependence would have no observable consequences. In practice, the series cannot be computed beyond the first two or three orders of perturbation theory for most observables. The truncated series do depend on renormalization prescription, and differ by terms of the leading uncomputed order in the series. Since $\alpha_s \sim 0.1-0.3$ at currently-accessible energy scales, the discrepancies are experimentally significant.

This type of dependence on the re-definition of a small expansion parameter will arise in any truncated series expansion. In particular, perturbative series in the fine structure constant α of Quantum electrodynamics (QED), are also subject to truncation ambiguities. The issue is less severe in QED however for two reasons: First, the expansion parameter $\alpha \simeq 1/137.034$ is much smaller than α_s , and so are truncation ambiguities. Secondly, there is a naturally preferred definition of α which is experimentally measurable in principle. In fact, the cross section for Compton scattering of a photon from a spin one-half charged particle can be shown to reduce to the classical Thompson cross section to all orders in perturbation theory in the limit of zero photon energy. There is no such natural definition in QCD, either in the low-energy limit where the theory becomes strongly interacting, or in the high-energy limit where the effective coupling tends to zero due to asymptotic freedom.

Several approaches have been proposed to deal with the prescription dependence of predictions in perturbative QCD:

- **Good universal prescriptions:** The strategy is to find and use a prescription that appears to give a reasonably convergent perturbation series in a wide variety of processes. The archetypical example of this approach is the widely-used $\overline{\text{MS}}$ scheme recommended by Bardeen, Buras, Duke and Muta[5] in which dimensionally-regularized quantities are renormalized by subtracting poles and certain associated constants in the combination

$$\frac{2}{4-N} + [\log(4\pi) - \gamma_E] , \quad (4)$$

where N is a continuation of 4 space-time dimensions and γ_E is Euler's constant. This is a modification of the minimal subtraction (MS) scheme of t'Hooft and Veltman[6] in which only the pole in $N - 4$ is subtracted. Another proposal by Brodsky, Lepage and Mackenzie[7] uses light-quark vacuum polarization insertions to determine the scale of α_s in any process that does not involve gluon-gluon couplings in leading order.

- **Fastest apparent convergence:** It is by no means guaranteed that a good universal prescription must exist. A different strategy suggested by Grunberg[8] tailors the prescription to each individual process in order to make the higher order terms in the series as small as possible. For example, in Eq. (3), one might choose $b'_n = 0$, so that the QCD prediction is given by the leading order term. The different coupling parameters, determined experimentally for example from the different moments M_n , are related to one another by Eqs. (2,3).
- **The principle of minimum sensitivity:** Stevenson[9] suggested choosing a renormalization prescription optimally for each process considered by requiring that the truncated perturbative expression be an extremum with respect to variations in the parameters of the renormalization group of Gell-Mann and Low[10], and Stueckelberg and Petermann[11]. At next-to-leading order in QCD, predictions depend on one renormalization group parameter, the scale μ of the effective coupling $\alpha_s(\mu)$.

Each of these strategies has its advantages and shortcomings. There is no rigorous justification for any of them within the framework of quantum field theory. Each of them is a more or less educated guess concerning the size of uncomputed terms in the perturbation series. The only way to verify this guess is to compute these unknown terms!

2.1 The momentum-space subtraction prescription

Celmaster and Gonsalves[2, 3] proposed an alternative to the MS and $\overline{\text{MS}}$ prescriptions called momentum-space subtraction (MOM). In this approach, one considers the basic off-shell Green's functions that must be renormalized in any perturbative calculation beyond tree level. At one-loop level, these are the three-gluon, the quark-gluon, and (in covariant gauges) the ghost-gluon scattering amplitudes. The theory is renormalized by subtracting these fundamental building-block amplitudes at an energy scale that is typical of the process under consideration, which also serves as the scale of the effective coupling α_s .

The motivation for the MOM prescription is the intuition that ultraviolet behavior is dominated by the off-shell Green's functions that need to be renormalized. If these Green's functions are primarily responsible for the divergent behavior of the unrenormalized theory, then subtracting their contributions at the typical energy scale of the process will minimize their effect on the perturbative correction terms. Because subtractions are performed on a small number of generic Green's functions, momentum-space subtraction is an example of a good universal prescription.

The MOM prescription proposal suffers from some ambiguities. There are three different vertices at one-loop level that can be chosen to define the subtraction. Each of these off-shell vertices is gauge dependent, and so a particular gauge must be chosen to define the subtraction. And finally, each three-point vertex has two independently-variable momenta flowing through it, and these must be fixed in relation to the energy scale.

A detailed study of these vertices showed that it is possible to define a class of MOM prescriptions that gives reasonably-sized next-to-leading order QCD corrections in a number of processes. The corrections are only weakly gauge-dependent if a covariant gauge is used with the gauge parameter allowed to vary quite freely in the range of the usual Feynman and Landau gauges. We choose a natural and intuitively reasonable choice of momenta at which to subtract a three-point function, namely the symmetric Euclidean point $p_1^2 = p_2^2 = p_3^2 = -\mu^2$. The off-shell Green's functions are related by Ward-Takahashi identities, which relate the different prescription in the MOM class to one another. For symmetric-point subtraction, the class of MOM prescriptions is also only weakly dependent on the chosen vertex.

2.2 The Celmaster-Gonsalves relation for Λ s in different schemes

Celmaster and Gonsalves[3] showed that Λ 's defined in different schemes can be related exactly by performing a one-loop calculation.

It is well known that the renormalization group equation

$$\mu \frac{dg(\mu)}{d\mu} = \beta(g(\mu)) = -\beta_0 g^3 - \beta_1 g^5 + \dots, \quad (5)$$

where β is the QCD beta function with leading coefficient $\beta_0 = 11 - 2n_f/3$, can be integrated to express the scale dependence of the QCD coupling

$$g^2(\mu) = \frac{1}{\beta_0 \log(\mu^2/\Lambda^2)} - \frac{\beta_1 \log \log(\mu^2/\Lambda^2)}{\beta_0^3 \log^2(\mu^2/\Lambda^2)} + \dots \quad (6)$$

in terms of a renormalization-group invariant QCD parameter Λ , which does however depend on the renormalization prescription used to define $g(\mu)$. This relation can be solved perturbatively for the ratio

$$\frac{\Lambda}{\Lambda'} = \exp \left[\frac{1}{2\beta_0} \left(\frac{1}{g'^2(\mu)} - \frac{1}{g^2(\mu)} \right) + \mathcal{O}(g^2) \right], \quad (7)$$

where the coupling parameters are related by Eq. (2). Because Λ and Λ' are scale-invariant constants, the limit $\mu \rightarrow \infty$ can be taken on the right hand side to give

$$\frac{\Lambda}{\Lambda'} = \exp \left[\frac{a}{\beta_0} \right], \quad (8)$$

where the constant a relates the two prescriptions in one-loop order. This result is *exact* to all orders in perturbation theory because of asymptotic freedom[12, 13] $g(\infty) = 0$.

The Celmaster-Gonsalves relation has been used to relate Λ_{Lattice} as measured in lattice QCD to $\Lambda_{\overline{\text{MS}}}$ determined from high energy phenomenology[14, 15].

3 QCD Radiative Corrections in Electron-Positron Annihilation

One of the most powerful probes of the short-distance structure of hadrons is the virtual photon produced by annihilation of an energetic pair in colliding beams of electrons and positrons. This process provides a plethora of measurable inclusive cross sections and distributions that have been used to discover new quark species, and to study bound states of heavy quarks, the densities of partons in hadrons, and the fundamental structure of the quark-gluon interaction. The simplest observable is the total cross section for annihilation to hadrons, which can be expressed in the form

$$\sigma(e^+e^- \rightarrow \text{hadrons}) = \frac{4\pi\alpha}{3E_{\text{cm}}^2} \left(\sum_f Q_f^2 \right) \left[1 + \frac{\alpha_s}{\pi} + K \left(\frac{\alpha_s}{\pi} \right)^2 + \dots \right], \quad (9)$$

where the sum is over quark flavors $f = u, d, s, c, b, t$, with Q_f being the fractional quark charge, and the next-to-leading order coefficient K is calculable in perturbative QCD. This simple form holds in regions far from flavor thresholds with the flavor sum being restricted to flavors with $4m_f^2 < E_{\text{cm}}^2$. The cross section is proportional to the number of quark colors and thus provides a direct measurement of the 3 in SU(3). The fractional electric charge of each new quark species is directly measured by the increase of the flavor sum as the threshold is crossed, and is most dramatically illustrated by the data in Fig. (1) on the ratio

$$R = \frac{\sigma(e^+e^- \rightarrow \text{hadrons})}{\sigma(e^+e^- \rightarrow \mu^+\mu^-)} = 3 \left(\sum_f Q_f^2 \right) \left[1 + \frac{\alpha_s}{\pi} + K \left(\frac{\alpha_s}{\pi} \right)^2 + \dots \right]. \quad (10)$$

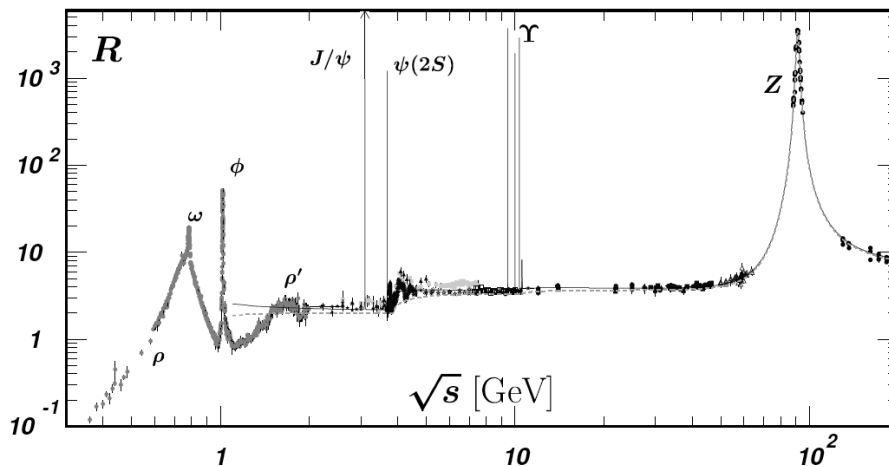


Figure 1: Data on the R ratio in e^+e^- annihilation from the PDG Review of Particle Physics[16].

The leading α_s/π correction was first computed by Schwinger[17]. The next-to-leading order coefficient K was computed analytically by Celmaster and Gonsalves[19, 20],

$$K_{\overline{\text{MS}}} = \frac{365}{24} - \frac{11}{12}n_f - 2\beta_0\zeta(3) \simeq 1.986 - 0.115n_f, \quad (11)$$

where ζ is Riemann's zeta function. This result agreed precisely with an earlier numerical calculation by Dine and Sapirstein[18] on gauge-invariant subsets of diagrams and their sum. The analytic result was also obtained in an independent calculation by Chetyrkin, Kataev and Tkachov[21].

The next-to-leading order coefficient can be expressed in other renormalization schemes using Eq. (2):

$$K_{\text{MOM}} = \frac{365}{24} - \frac{85}{36\sqrt{3}}\text{Cl}_2\left(\frac{\pi}{2}\right) - \frac{23}{36}n_f - 2\beta_0\zeta(3) \simeq -2.193 + 0.162n_f, \quad (12)$$

$$K_{\overline{\text{MS}}} = \frac{365}{24} - \frac{11}{12}n_f + \frac{\beta_0}{2}[\log(4\pi) - \gamma_E - 4\beta_0\zeta(3)] \simeq 7.359 - 0.441n_f, \quad (13)$$

where Cl is Clausen's function, and the MOM scheme is defined by the quark-quark-gluon vertex in Landau gauge. Note that MOM and $\overline{\text{MS}}$ give a well-behaved perturbation series. The simple MS scheme is less well behaved.

The theoretical prediction for R has since been extended to $\mathcal{O}(\alpha_s^3)$ by Gorishnii, Kataev and Larin[26], and Surguladze and Samuel[27], and work is in progress[28] on the $\mathcal{O}(\alpha_s^4)$ coefficient.

3.1 The photon propagator in QCD

The total annihilation cross section can most easily be obtained from the 2-point correlation function for the electromagnetic vector potential

$$D_{\mu\nu}(q) = \int dx e^{iq \cdot x} \langle T[A_\mu(x)A_\nu(0)] \rangle = \frac{-i}{q^2} \left(g_{\mu\nu} - \frac{q_\mu q_\nu}{q^2} \right) D(-q^2) + \text{gauge terms}. \quad (14)$$

The total cross section is given by the imaginary part of the photon propagator

$$\sigma(e^+e^- \rightarrow \text{hadrons}) = -\frac{4\pi\alpha}{q^2} \Im D(-q^2), \quad (15)$$

with $q^2 = E_{\text{c.m.}}^2$.

If QCD with massless quarks were a finite theory, then the dimensionless function $D(-q^2)$ would be a pure number independent of q^2 . Because of ultraviolet and infrared divergences, the theory must be regularized to compute $D(-q^2)$ as a perturbative series in the QCD coupling α_s . This is most conveniently done by analytically continuing $D(-q^2)$ to the region of spacelike $q^2 < 0$ and to space-time dimension $N = 4 - \epsilon$. The unrenormalized function D is then real and finite, with divergences manifest as poles in ϵ

$$D(-q^2) = 1 + \frac{\alpha_0}{\pi} \sum_{n=1}^{\infty} (-q^2)^{-n\epsilon} d_n(\epsilon) \left(\frac{\alpha_{s0}}{\pi} \right)^{n-1} + \mathcal{O}(\alpha_0^2), \quad (16)$$

where α_0 and α_{s0} are the unrenormalized (bare or zero order) QED and QCD coupling parameters respectively, and the coefficient

$$d_n = \frac{d_{n,n}}{\epsilon^n} + \frac{d_{n,n-1}}{\epsilon^{n-1}} + \dots + \frac{d_{n,1}}{\epsilon} + d_{n,0} + \mathcal{O}(\epsilon), \quad (17)$$

is got by computing n -loop Feynman diagram contributions to the photon propagator. The dependence of the unrenormalized propagator on the sole dimensional quantity q^2 in massless QCD follows from dimensional analysis.

The propagator is made finite in the limit $\epsilon \rightarrow 0$ by subtracting divergences at a renormalization scale μ . The bare QCD coupling α_{s0} is then replaced by the effective couple $\alpha_s(\mu)$. Since the electromagnetic current is conserved, the bare QED coupling α_0 can simply be replaced by its renormalized value (which differs from the usual fine structure constant α by terms of order α^2). It is then straightforward to express the coefficient K in Eq. (9) in terms of the residues of the poles in Eq. (17).

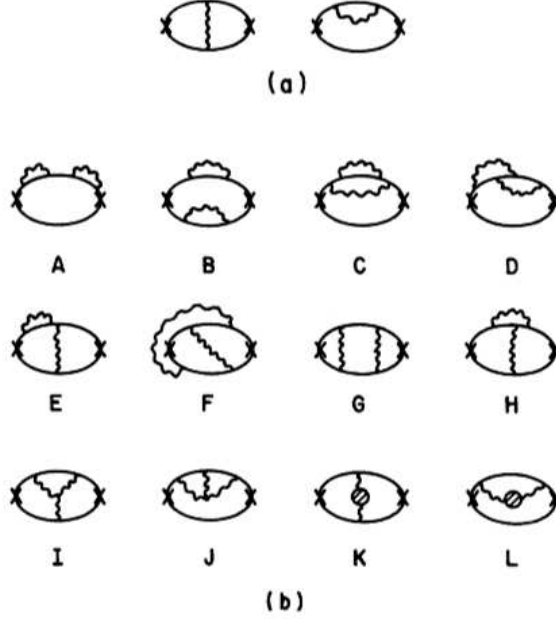


Figure 2: Feynman diagrams which contribute to the photon propagator in QCD through order α_s^2 .

3.2 The Gegenbauer expansion technique

The residues $d_{n,i}$ in Eq. (17) were computed by evaluating the Feynman diagrams in Fig. (2) assuming massless quarks and using dimensional regularization. The calculation was done by generalizing a well-known Chebyshev polynomial expansion technique developed by Rosner and others[22, 24] for QED to N -dimensions. The appropriate generalization is provided by Gegenbauer polynomials $C_n^\lambda(x)$ with $\lambda = (N-2)/2$ and x the cosine of the polar angle in N -dimensional spherical coordinates.

The Gegenbauer polynomials[23] can be generated from $C_0^\lambda = 1$ using the recursion formula

$$2(n + \lambda)x C_n^\lambda(x) = (n + 1)C_{n+1}^\lambda(x) + (1 - \delta_{n,0})(n + 2\lambda - 1)C_{n-1}^\lambda(x), \quad (18)$$

and obey the orthogonality relation

$$\int_{-1}^{+1} dx (1 - x^2)^\lambda C_n^\lambda(x) C_m^\lambda(x) = \delta_{n,m} \frac{\pi 2^{1-2\lambda} \Gamma(n + 2\lambda)}{n!(n + \lambda) [\Gamma(\lambda)]^2}. \quad (19)$$

The basic idea is to expand propagator denominators of massless quarks or gluons using an N -dimensional generalization of the Legendre polynomial expansion

$$\frac{1}{(\vec{k}_1 - \vec{k}_2)^2} = \frac{1}{k_>^2} \sum_{n=0}^{\infty} f_n \left(\frac{k_<}{k_>} \right) C_n^\lambda(\hat{k}_1 \cdot \hat{k}_2), \quad (20)$$

where the coefficient functions f_n are related to hypergeometric functions and can be expressed as a power series in the dimensional regularization parameter ϵ

$$f_n(x) = x^n \left[1 + \frac{\epsilon}{2} \left\{ (1 - \delta_{n,0}) \sum_{j=1}^n \frac{1}{j} + (n + 1) \sum_{j=1}^{\infty} \frac{x^j}{j(n + j + 1)} \right\} + \mathcal{O}(\epsilon^2) \right]. \quad (21)$$

Integrations over loop momenta can then be performed using the orthogonality relation in Eq. (19) and various other properties of the Gegenbauer polynomials.

The calculation of Chetrykin, Kataev and Tkachov[21] used a similar polynomial expansion technique in position space[25].

4 The Quark Electromagnetic Form Factor in QCD

A different method for computing the total annihilation cross section discussed in the preceding section would be to calculate the amplitudes for a virtual photon to decay to 2, 3, or 4 partons, and then sum the individual cross sections integrated over the phase space of final state partons. Fig. (3) shows the Feynman diagrams which contribute to the 2-parton final states through order α_s^2 , i.e., to the quark electromagnetic form factor.

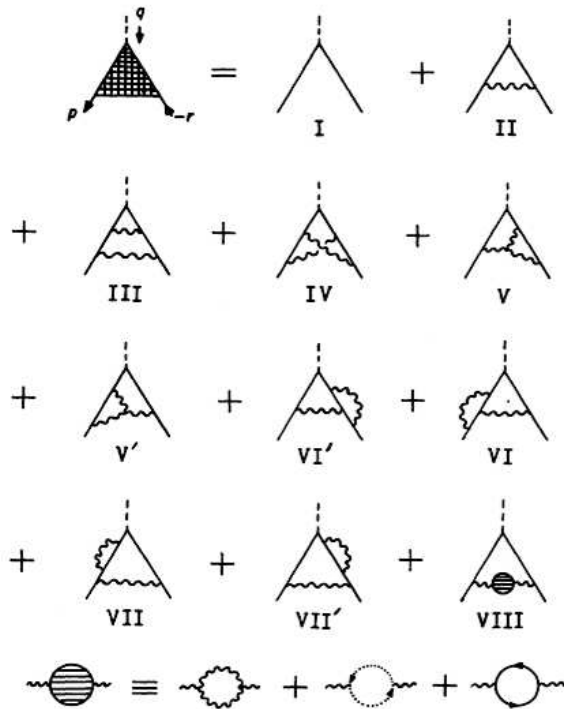


Figure 3: One-particle irreducible Feynman diagrams which contribute to the quark electromagnetic form factor in QCD. Solid, wavy, and dashed lines represent quark, gluon, and ghost propagators, respectively. Diagram IV is the only non-planar diagram in this set.

The form factor is ultra-violet finite (when all QCD counterterms are included) because the electromagnetic current is conserved, but it is infrared divergent due to soft and collinear singularities. These singularities are canceled by contributions from 3- and 4-parton final states so the total cross section is finite. The form factor is therefore an unphysical part of a measurable physical observable. However, it is an object of great theoretical interest because the soft and collinear singularities are generic in that they determine double-logarithmic Sudakov effects in many measurable cross section—see the review article by Collins[29]. It was therefore of interest to study these singularities.

A calculation[30] of all two-loop integrals required for an analytical calculation of the form factor was completed in 1983, including all terms of $\mathcal{O}(\epsilon^{-n})$ with $0 \leq n \leq 4$. The most challenging sets of integrals to compute were those which contribute to the box-plus-triangle diagram III and the non-planar diagram IV in Fig. (3). The calculations were done by converting the two-loop momentum integrals to 5-dimensional

integrals over Feynman parameters. The Feynman parameter integration were performed analytically in succession using various techniques including infinite-series expansion of binomial expressions where necessary. Care had to be taken to ensure that the binomial expansions converged after each successive integration: where necessary, the integration interval was subdivided and appropriately converging expansions used in each region.

The results for the two-loop scalar integrals were verified by van Neerven[31] and by Kramer and Lampe[32]. Gehrmann, Huber and Maitre[33] have recently obtained elegant exact expressions for the integrals in diagram IV in N dimensions.

These two-loop results have been used in several $\mathcal{O}(\alpha_s^2)$ QCD calculations including the Drell-Yan total cross section by Hamberg, van Neerven and Matsuura[34], the total cross section for Higgs production by Harlander and Kilgore[35] and Anastasiou and Melnikov[36], the Drell-Yan rapidity distribution by Anastasiou, Dixon, Melnikov and Petriello[37], and the Higgs total cross section and Drell-Yan and Higgs rapidity distributions by Ravindran, Smith and van Neerven[38].

In a closely related calculation[39], a tensor decomposition scheme that is exact in N dimensions was used to compute the one-loop QCD corrections to the e^+e^- total annihilation cross section. Unlike the process $\gamma^* \rightarrow q\bar{q}$ in which there is a single scalar form factor, the process $\gamma^* \rightarrow q\bar{q}g$ involves 6 independent invariant tensors and corresponding form factors in $N = 4$ dimensions. When the amplitude is continued to N dimensions, there is a set of 17 linearly-independent tensors and corresponding form factors into which it can conveniently be decomposed. The decomposition makes it possible to compute the dimensionally-regularized amplitude very efficiently in $\mathcal{O}(\alpha_s)$, and the technique readily extends to two or more loops.

Over the past few years, a number of results on form factors have appeared in the literature, including analytic results for arbitrary masses and momenta in QED[40, 41] and in QCD[42], and impressive new results on massless quark and gluon form factors at three loops[43].

5 Chromo-Electroweak Interference and Parity Violation

In the Standard Model the process $q\bar{q} \rightarrow q\bar{q}V$ (where $V = W^\pm, Z^0$ or γ) can occur via gluon exchange and also via W^\pm or Z^0 exchange. The corresponding chromodynamic and electroweak amplitudes can interfere with one another[44] as shown in Fig. (4). These interference cross sections are largest when the exchanged W^\pm or Z^0 is on-shell when they are also odd under parity. Interference cross sections computed using helicity-amplitude techniques were analyzed[45] for all interesting subprocesses as well as for the processes $q\bar{q} \rightarrow q\bar{q}l\bar{l}$ in which the lepton pair $l\bar{l}$ comes from the decay of V on-shell. Parity-violating asymmetries were defined and presented at the parton level and for the hadronic processes pp or $p\bar{p} \rightarrow V + 2$ jets or $l\bar{l} + 2$ jets, see Fig. (5). These asymmetries are independent of the polarizations of all particles involved, and do not require that the flavors of the jet partons be measured. They are generally of order 0.01 pb at energies $\sqrt{s} \gtrsim 1$ TeV.

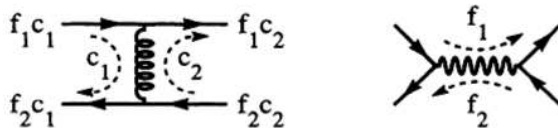


Figure 4: A solid line represents a quark or antiquark with color c and flavor f . The wavy line represents a color-neutral electroweak boson and the curly line a flavor-neutral gluon. The two amplitudes can interfere because their initial states (on the left) can have identical quantum numbers as can their final states (on the right).

A simple way of defining experimental observables that are sensitive to this parity-odd character of the interference terms is as follows: Imagine that the incident beams lie in the plane of a mirror, as in Fig. (6). If the incident beams are not polarized, the initial state is invariant under reflection in this mirror. We will

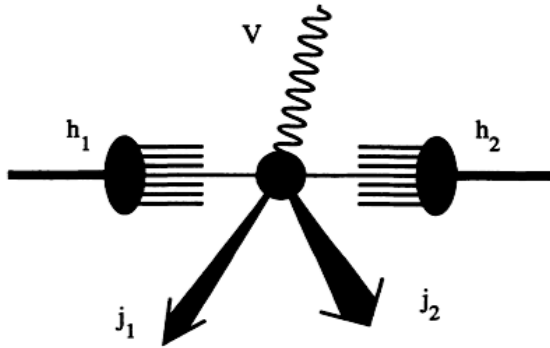


Figure 5: Hadrons h_1 and h_2 collide to produce an on-shell electroweak boson V and two hadron jets j_1 and j_2 at large transverse momentum.

also assume that the spins of the final state particles are not detected, i.e., particles are identified by their momenta and internal quantum numbers only. A parity-odd contribution to the cross section can make the probabilities for observing a particular event (i.e., a particular configuration of final state particles) and its mirror image different from one another. Since the events are continuously distributed in phase space, the likelihood of finding an event and its geometrical mirror image in any finite sample of events is vanishingly small. To decide experimentally whether or not there is an asymmetry with respect to mirror reflection in the event sample, one must count the number of events that fall in some region of phase space (which we will call a “bin”) and the number of events that fall in the mirror image of this region (which we will call the “image bin”) and then decide whether or not there is a statistically significant difference between these two numbers. This difference can be compared with a “parity-violating asymmetry” which we define as follows:

$$a^{\text{PV}}(\text{bin}) = \int_{\text{bin}} d\sigma - \int_{\text{image bin}} d\sigma . \quad (22)$$

The integral over the bin includes an implicit sum over all final state quantum numbers that are not observed, i.e., color quantum numbers and any spin or flavor quantum numbers that cannot be experimentally measured.

A set of bins will have to be judiciously chosen to maximize the observed effects of parity violation, i.e., to yield the largest cumulative asymmetry. Thus we also define a cumulative parity-violating asymmetry as follows:

$$A^{\text{PV}} = \sum_{\text{bins}} | a^{\text{PV}}(\text{bin}) | , \quad (23)$$

where the sum is taken over bins that do not overlap with one another. A theoretical upper bound on A^{PV} is given by

$$A_{\text{max}}^{\text{PV}} = \sum_{\text{bins}} \lim_{\text{bin size} \rightarrow 0} | a^{\text{PV}}(\text{bin}) | \quad (24)$$

$$= \frac{1}{2} \int_{\langle \text{cuts} \rangle} d\Omega \left| \left(\frac{d\sigma}{d\Omega} \right) - \left(\frac{d\sigma}{d\Omega} \right)_{\text{mirror image}} \right| . \quad (25)$$

These asymmetries might be observable in pp and $p\bar{p}$ collisions above the threshold for production of pairs of electroweak bosons, i.e., at center of mass energies in the TeV range and these asymmetries are comparable in magnitude to the pair-production cross sections. Fig. (7) compares the parity-violating signal with the

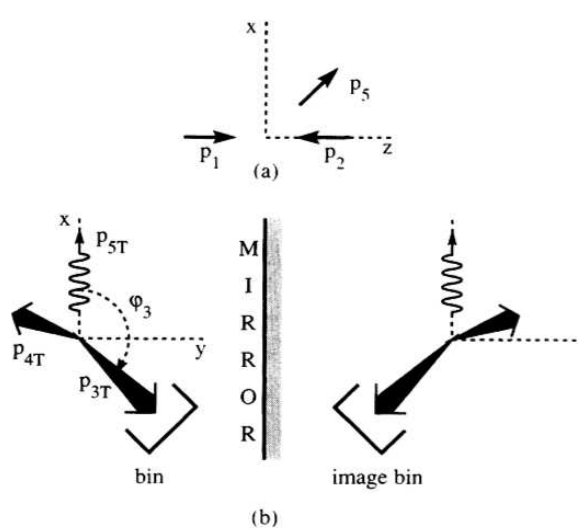


Figure 6: (a) Momenta in the $x-z$ plane. p_1 is the momentum of the quark (parton-level asymmetry), the proton ($p\bar{p}$ collisions), or one of the protons chosen arbitrarily (pp collisions). p_5 is the momentum of $V = W^\pm, Z^0$ (3-particle final state) or of the lepton (4-particle final state). A right-handed coordinate system is defined such that $p_5^x > 0$ and $p_5^y = 0$. (b) Momenta in the $x-y$ plane. p_3 and p_4 are the momenta of the two jet partons. Parity is violated if the event shown on the left and its mirror image shown on the right occur with different probabilities.

QCD background[59] in $W + 2$ jet production. Unlike the W -pair production cross section which is parity conserving, the interference contribution is parity-violating, and this might make it easier to observe above a rather formidable QCD background of electroweak boson + 2 jet events. Actual observation of these effects will require somewhat higher integrated luminosities than are currently available for example at the Tevatron at Fermilab. It remains to be seen whether these subtle Standard Model predictions will be observable at a high-energy multi-TeV hadron collider such as the LHC. Analogous parity-violating signatures may also be observable in electron-positron annihilations[46] at the ILC.

6 Electroweak Boson Production at Large Transverse Momentum

The production of electroweak bosons at large transverse momentum is one of the most important processes at current and future hadron colliders. The QCD-improved parton model predicts that if the intrinsic energy scale involved is sufficiently large, the inclusive cross section for the process

$$h_1(P_1) + h_2(P_2) \rightarrow V(Q) + X, \quad (26)$$

where h_i , $i = 1, 2$ are unpolarized hadrons with momenta P_i , can be reliably computed using the following approximate factorized form:

$$E_Q \frac{d\sigma}{d^3Q} = \sum_{a_1, a_2} \int_0^1 dx_2 dx_1 f_{a_1}^{h_1}(x_1, M^2) f_{a_2}^{h_2}(x_2, M^2) E_Q \frac{d\sigma^{a_1 a_2}}{d^3Q}(x_1 P_1, x_2 P_2, M^2). \quad (27)$$

Here $E_Q \equiv Q^0$, a and b stand for quarks, antiquarks or gluons, $f_a^h(x, M^2)$ is the probability density for finding parton a with momentum fraction x in hadron h if it is probed at scale M^2 , and $\sigma^{ab}(p_1, p_2, M^2)$ is the perturbative cross section for the process

$$a(p_1) + b(p_2) \rightarrow V(Q) + X, \quad (28)$$

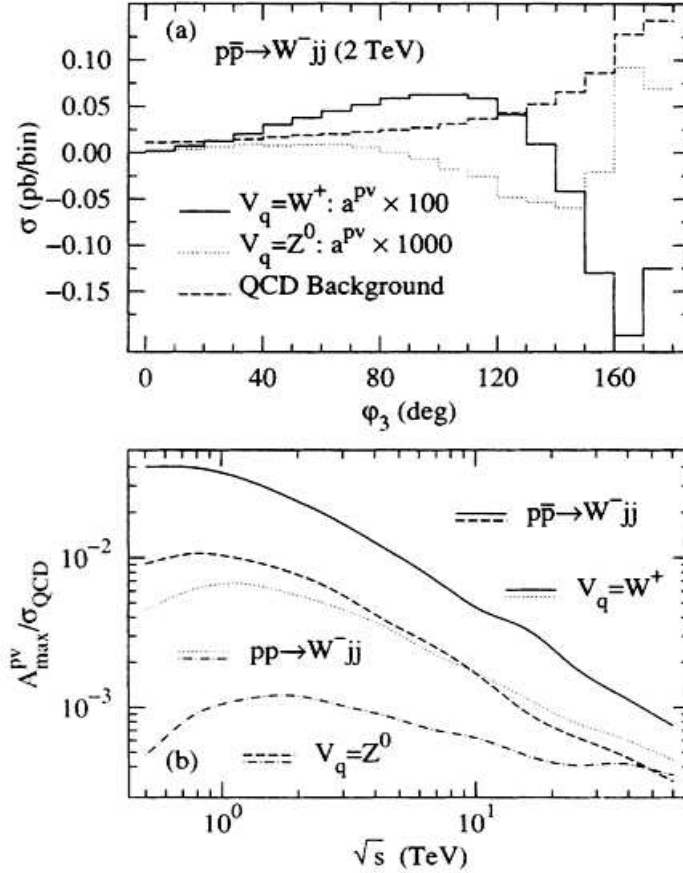


Figure 7: Comparison of signal to background in $W^- + 2$ jet production. (a) Binned cross sections with $200 \text{ GeV} < \sqrt{s_{12}} < 600 \text{ GeV}$. The parity-violating asymmetries have been multiplied by the factors (100 and 1000) indicated to show them on the same scale as the QCD background. (b) Variation of the signal to background ratio in pp and $p\bar{p}$ collisions as a function of the colliding beam energy.

from which collinear singularities arising from radiation off massless partons have been factorized out at scale M^2 and implicitly included in the scale-dependent parton densities $f_a^h(x, M^2)$.

A complete analytical calculation of the next-to-leading order QCD radiative corrections to the inclusive cross sections $parton + parton \rightarrow V + X$, where V is an on-shell W^\pm or Z^0 with transverse momentum Q_T of order M_W , or a massive virtual photon with Q_T of order of its invariant mass, was done by Gonsalves, Pawłowski and Wai[48] and by Arnold and Reno[49]. This work completed an earlier calculation by Ellis, Martinelli and Petronzio[47] of the non-singlet (NS) contributions to lepton-pair production at large Q_T . Numerical predictions for W , Z and γ^* production at collider energies were computed, and the dependence of the radiative corrections on the choice of renormalization and factorization scales was studied. Results[50] on varying the renormalization and factorization scales independently were used to compare the FAC[8] and PMS[9] prescriptions. These results showed that the QCD-improved parton model can be used to make firm and reliable predictions for electroweak boson production at large Q_T .

In Fig. (8), the theoretical predictions are compared with measurements[51, 52] of the W transverse momentum distributions by the UA1 and UA2 collaborations at the CERN Sp \bar{p} S collider. It is clear that data are consistent with the QCD predictions, but that they are not accurate enough to discriminate between

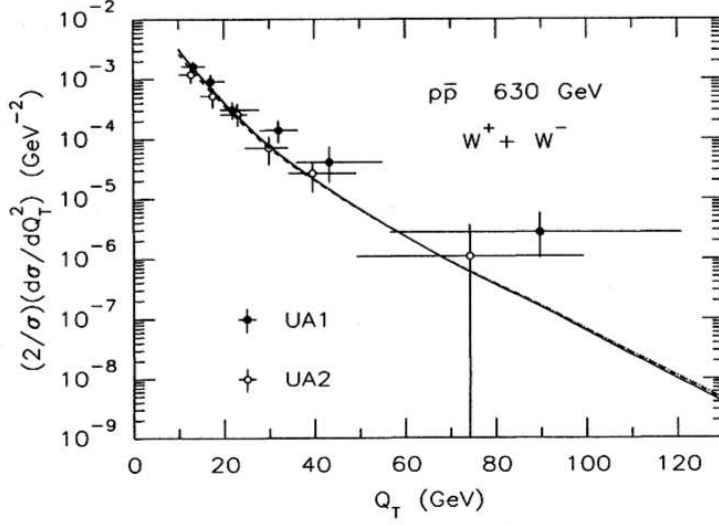


Figure 8: W production in $p\bar{p}$ collisions at 630 GeV. The solid, dashed, and dotted lines represent the Full (MRSB), Full (MRSE), and NS (MRSB) predictions. The corresponding total cross sections σ are 5.8, 5.1, and 3.5 nb, respectively.

the MRSB and MRSE distributions[53] or between the singlet and non-singlet theoretical predictions. There is a tantalizing, but statistically insignificant, hint in the data that the experimental cross section might be larger than the theoretical prediction at large values of Q_T .

Fig. (9) shows a comparison of theoretical predictions with experimental measurements by the D0 Collaboration. The theoretical results in this figure have been improved at small Q_T by resumming Sudakov logarithms of Q_T^2/M_W^2 . The data are completely consistent with the predictions and there is no evidence in the tail of the distribution for new physics beyond the Standard Model at large Q_T .

6.1 Large logarithmic soft-gluon corrections

Predictions for the W transverse momentum distribution at next-to-leading order (NLO) in α_s and including the next-to-next-to-leading order (NNLO) soft-gluon corrections at LHC energies were presented recently by Gonsalves, Kidonakis and Sabio-Vera[55].

Let s_2 be the invariant mass of the final state partons recoiling against the W boson. In general, the partonic cross section $\hat{\sigma}$ includes distributions with respect to s_2 at n -th order in the QCD coupling α_s of the type

$$\left[\frac{\ln^m(s_2/Q_T^2)}{s_2} \right]_+, \quad m \leq 2n - 1, \quad (29)$$

defined by their integral with any smooth function f by

$$\int_0^{s_2 \max} ds_2 f(s_2) \left[\frac{\ln^m(s_2/Q_T^2)}{s_2} \right]_+ \equiv \int_0^{s_2 \max} ds_2 \frac{\ln^m(s_2/Q_T^2)}{s_2} [f(s_2) - f(0)] + \frac{1}{m+1} \ln^{m+1} \left(\frac{s_2 \max}{Q_T^2} \right) f(0). \quad (30)$$

These “plus” distributions are the remnants of cancellations between real and virtual contributions to the cross section. Let us make use of the terminology that at n -th order in α_s the leading logarithms (LL)

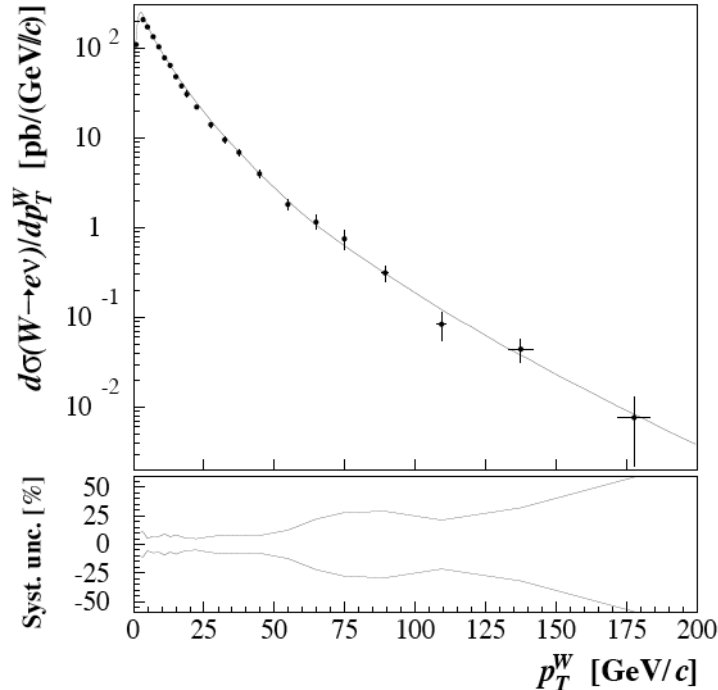


Figure 9: W production in $p\bar{p}$ collisions at 1.8 TeV measured by the D0 Collaboration[54].

are those with $m = 2n - 1$ in Eq. (29), the next-to-leading logarithms (NLL) are those with $m = 2n - 2$, the next-to-next-to-leading logarithms (NNLL) are those with $m = 2n - 3$, and the next-to-next-to-next-to-leading logarithms (NNNLL) are those with $m = 2n - 4$. The symbol “NNLO-NNNLL” means that soft-gluon contributions through NNNLL to the NNLO corrections have been included and added to the complete NLO result.

Fig. (10) shows the differential cross section $d\sigma/dQ_T^2$ at high Q_T with $\sqrt{S} = 14$ TeV for the two scale values, $Q_T/2$ and $2Q_T$, often used to display the uncertainty due to scale variation. Note that while the variation of the Born cross section is significant and the variation at NLO is similar to LO, at NNLO-NNNLL it is very small. In fact the two NNLO-NNNLL curves lie very close to or on top of each other. With this calculation, reliable predictions of perturbative QCD, including soft-gluon effects, for the W transverse momentum distribution are available and await comparison with experimental measurements at the LHC in the near future. Any deviation from these predictions would be an unambiguous signal of new physics beyond the Standard Model.

It is obviously worthwhile to compute the complete NNLO corrections to the transverse momentum distribution. This would further reduce the scale dependence of the predictions, and it would also provide information on soft and logarithms at $\mathcal{O}(\alpha_s^4)$. Fixed order QCD calculations for analogous processes in e^+e^- annihilation have been completed over the past few years, see e.g. Gehrmann-De Ridder et al.[56], and references therein. An $\mathcal{O}(\alpha_s^3)$ calculation at finite Q_T would require the two-loop corrections to subprocesses such as $q\bar{q} \rightarrow Wg$, one-loop corrections to subprocesses such as $q\bar{q} \rightarrow Wgg$, and tree-level amplitudes such as $q\bar{q} \rightarrow Wggg$.

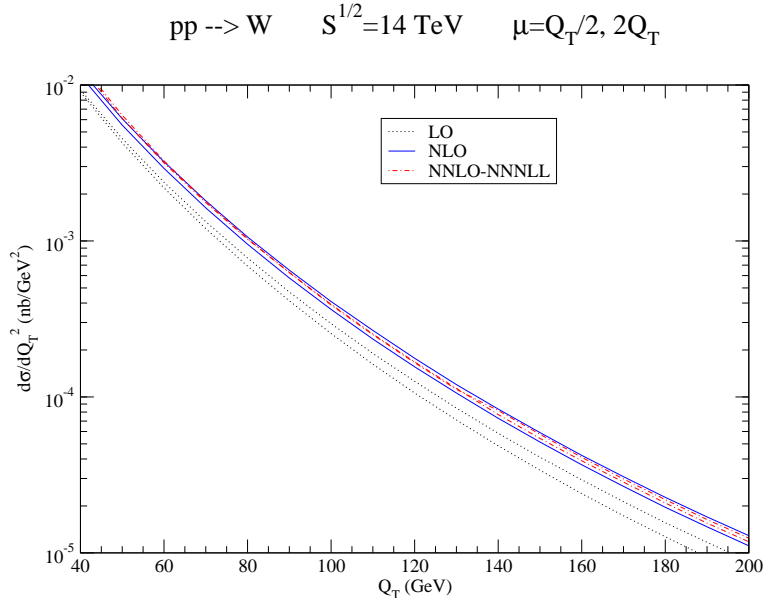


Figure 10: The differential cross section, $d\sigma/dQ_T^2$, for W production in pp collisions at the LHC with $\sqrt{S} = 14$ TeV and $\mu = \mu_F = \mu_R = Q_T/2$ or $2Q_T$. Shown are the LO, NLO, and NNLO-NNLL results using the MRST 2002 LO, NLO and NNLO parton distributions[63]. The upper lines are with $\mu = Q_T/2$, the lower lines with $\mu = 2Q_T$.

7 Heavy Quark Triangle Diagram Contributions at High Energies

Because the masses of the W and Z bosons are large compared with the masses of the quark and gluon constituents in the colliding hadrons, it is generally a good approximation to assume that the quarks are massless in computing the production cross sections for these electroweak bosons at high energies. An exception, of course is the top quark, whose mass $m_t = 174$ GeV, is approximately twice as large as that of the W or Z .

The top quark can contribute to production amplitudes in three ways: as an initial state partonic constituent of one of the colliding hadrons, as an on-shell particle in the final state, and as a virtual particle. The density of top quarks in the colliding hadrons can safely be neglected. The production of real top quarks can safely be treated in a threshold approximation with the mass taken to be infinite below threshold and zero above. Top quarks in loops pose a delicate problem because the Standard Model is renormalizable only if the left-handed quarks occur in $SU(2)_L$ doublets. This requirement is imposed by the well-known triangle anomaly (which was discovered in QED by Adler[57] and Bell and Jackiw[58]) in the effective coupling of the axial-vector current to two gluons: if the top quark is omitted from the loop the amplitude is divergent in a non-renormalizable way; if the top quark is included and assumed massless the top and bottom contributions cancel; and if the top quark is included with a finite mass the contribution grows as the logarithm of the ratio of top to bottom masses.

The contributions in second order QCD of the diagrams in the left panel of Fig. (11) involving a heavy-quark triangle with vector, vector and axial-vector vertices were studied by Gonsalves, Hung and Pawłowski[61]. The contributions from the process $q\bar{q} \rightarrow Zgg$ ((a) in Fig. (11)) had been analyzed earlier by Dicus and Willenbrock[60], who concluded that the contributions were numerically small at Tevatron energies. The right panel of Fig. (11) shows the numerical magnitudes of the various subprocess contributions at Tevatron energies.

Rijken and van Neerven[62] subsequently computed all heavy quark contributions to the W and Z

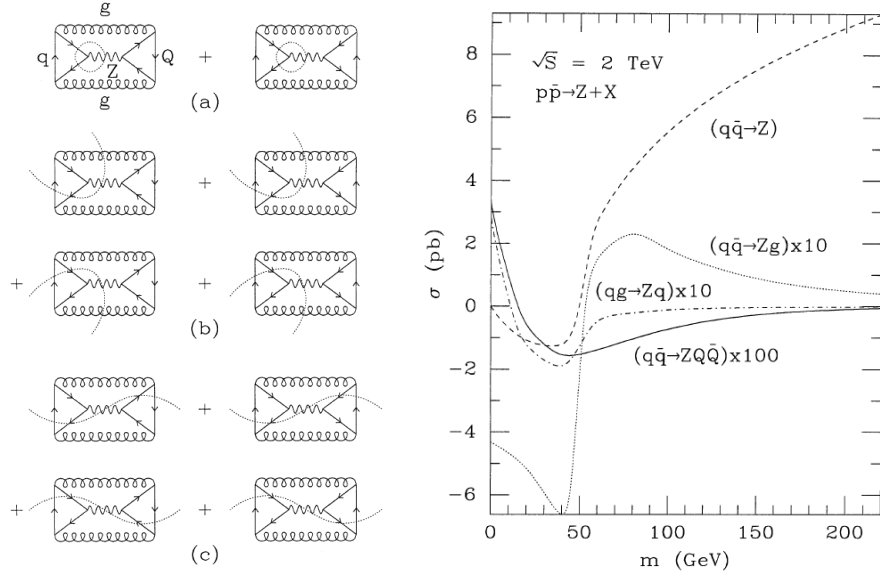


Figure 11: Left panel: Diagrams which contribute to the total cross section for producing a Z boson in hadron collisions. Q and q represent heavy and massless quarks, respectively, and g a gluon. Propagators cut by a dotted line are taken to be on shell in the initial or final state. Right panel: Contributions from heavy-quark triangle diagrams to the total cross section for Z production in $p\bar{p}$ collisions at 2 TeV. m is the mass of the heavy quark, which is assumed to have weak isospin $+\frac{1}{2}$. A quark with weak isospin $-\frac{1}{2}$ would contribute with opposite sign. The total cross section at 2 TeV is approximately 5 nb.

total cross sections, neglecting only diagrams with heavy quarks in the initial state. They found that the contributions from the top quark were negligible at Tevatron energies, but would contribute significantly at LHC energies with magnitude comparable to the $\mathcal{O}(\alpha_s^2)$ QCD corrections.

It is important to evaluate the top-quark-mass contributions to other measurable cross sections at LHC energies, in particular the W and Z transverse momentum distributions. Fig. (12) shows the Z transverse-momentum distribution at Tevatron and LHC energies including quark-triangle diagrams shown in Fig. (11). Quark masses are taken into account using a simple threshold prescription[48] by inserting a step function $\theta(Q_T^2 - 4m_f^2)$ into sums over quark flavors f in the subprocess cross sections. There is a significant change in the shape of the distribution at LHC energies due specifically to the virtual triangle-anomaly diagrams.

Because the triangle-anomaly contributions are comparable in magnitude to the $\mathcal{O}(\alpha_s^2)$ QCD radiative corrections, it is essential to include the top and bottom quark masses in the virtual triangle diagrams. A more precise calculation of the triangle-anomaly contributions to the Z transverse momentum distribution at LHC energies will be published elsewhere.

Acknowledgements

I would like to acknowledge my collaborators, W. Celmaster, C.W. Choi, R.K. Ellis, C.M. Hung, N. Kidonakis, J. Pawłowski, S. Raina, A. Sabio-Vera, and C.F. Wai, without whose collaboration many of the calculations described here would not have been possible. I am grateful to the National Science Foundation for support over many years, most recently through NSF-PHY-92-12177, as well as support provided by the Center for Computational Research at the University at Buffalo.

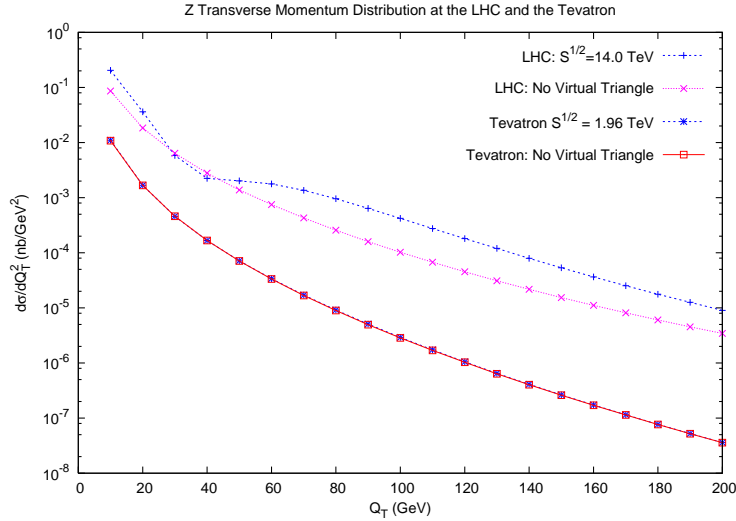


Figure 12: Z production at the LHC and the Tevatron. The data points represent NLO predictions computed using MRST 2002 NLO parton distributions[63]. Note the change in shape of the distribution at LHC energies (upper curves) compared with Tevatron energies (lower curves) when the anomaly diagrams are included. The anomalous contributions are negligibly small at the Tevatron.

References

- [1] P. L. Jain, G. Singh and R. Gonsalves, *Mod. Phys. Lett. A* **12** (1997) 1101.
- [2] W. Celmaster and R. J. Gonsalves, *Phys. Rev. Lett.* **42** (1979) 1435.
- [3] W. Celmaster and R. J. Gonsalves, *Phys. Rev. D* **20** (1979) 1420.
- [4] R. K. Ellis, W. J. Stirling and B. R. Webber, *QCD and Collider Physics* (Cambridge University Press, Cambridge, 1996).
- [5] W. A. Bardeen, A. J. Buras, D. W. Duke and T. Muta, *Phys. Rev. D* **18** (1978) 3998.
- [6] G. 't Hooft and M. J. G. Veltman, *Nucl. Phys. B* **44**, 189 (1972).
- [7] S. J. Brodsky, G. P. Lepage and P. B. Mackenzie, *Phys. Rev. D* **28** (1983) 228.
- [8] G. Grunberg, *Phys. Lett. B* **95** (1980) 70; Erratum *ibid.* B **110** (1982) 501.
- [9] P. M. Stevenson, *Phys. Rev. D* **23** (1981) 2916.
- [10] M. Gell-Mann and F. E. Low, *Phys. Rev.* **95** (1954) 1300.
- [11] E. C. G. Stueckelberg and A. Petermann, *Helv. Phys. Acta* **26** (1953) 499.
- [12] D. J. Gross and F. Wilczek, *Phys. Rev. Lett.* **30** (1973) 1343.
- [13] H. D. Politzer, *Phys. Rev. Lett.* **30** (1973) 1346.
- [14] A. Hasenfratz and P. Hasenfratz, *Phys. Lett. B* **93** (1980) 165.
- [15] R. F. Dashen and D. J. Gross, *Phys. Rev. D* **23** (1981) 2340.

- [16] W. M. Yao *et al.* [Particle Data Group], J. Phys. G **33** (2006) 1.
- [17] J. S. Schwinger, Phys. Rev. **74** (1948) 1439.
- [18] M. Dine and J. R. Sapiirstein, Phys. Rev. Lett. **43** (1979) 668.
- [19] W. Celmaster and R. J. Gonsalves, Phys. Rev. Lett. **44** (1980) 560.
- [20] W. Celmaster and R. J. Gonsalves, Phys. Rev. D **21** (1980) 3112.
- [21] K. G. Chetyrkin, A. L. Kataev and F. V. Tkachov, Phys. Lett. B **85** (1979) 277.
- [22] E. De Rafael and J. L. Rosner, Annals Phys. **82** (1974) 369.
- [23] M. Abramowitz and I. A. Stegun, *Handbook of Mathematical Functions* (Dover, New York, 1972)
- [24] M. J. Levine and R. Roskies, Phys. Rev. D **9** (1974) 421.
- [25] A. A. Vladimirov, Theor. Math. Phys. **43** (1980) 417 [Teor. Mat. Fiz. **43** (1980) 210].
- [26] S. G. Gorishnii, A. L. Kataev and S. A. Larin, Phys. Lett. B **212** (1988) 238.
- [27] L. R. Surguladze and M. A. Samuel, Phys. Rev. Lett. **66** (1991) 560; Erratum *ibid.* **66** (1991) 2416.
- [28] P. A. Baikov, K. G. Chetyrkin and J. H. Kuhn, Nucl. Phys. Proc. Suppl. **157** (2006) 27 [arXiv:hep-ph/0602126].
- [29] J. C. Collins, Adv. Ser. Direct. High Energy Phys. **5** (1989) 573 [arXiv:hep-ph/0312336].
- [30] R. J. Gonsalves, Phys. Rev. D **28** (1983) 1542.
- [31] W. L. van Neerven, Nucl. Phys. B **268** (1986) 453.
- [32] G. Kramer and B. Lampe, J. Math. Phys. **28** (1987) 945.
- [33] T. Gehrmann, T. Huber and D. Maitre, Phys. Lett. B **622** (2005) 295 [arXiv:hep-ph/0507061].
- [34] R. Hamberg, W. L. van Neerven and T. Matsuura, Nucl. Phys. B **359** (1991) 343 Erratum, *ibid.* B **644** (2002) 403.
- [35] R. V. Harlander and W. B. Kilgore, Phys. Rev. Lett. **88** (2002) 201801 [arXiv:hep-ph/0201206].
- [36] C. Anastasiou and K. Melnikov, Nucl. Phys. B **646**, 220 (2002) [arXiv:hep-ph/0207004].
- [37] C. Anastasiou, L. J. Dixon, K. Melnikov and F. Petriello, Phys. Rev. D **69** (2004) 094008 [arXiv:hep-ph/0312266].
- [38] V. Ravindran, J. Smith and W. L. van Neerven, Nucl. Phys. B **665**, 325 (2003) [arXiv:hep-ph/0302135]; Nucl. Phys. B **767**, 100 (2007) [arXiv:hep-ph/0608308].
- [39] R. J. Gonsalves, Phys. Rev. D **34** (1986) 1316.
- [40] P. Mastrolia and E. Remiddi, Nucl. Phys. B **664** (2003) 341 [arXiv:hep-ph/0302162].
- [41] R. Bonciani, P. Mastrolia and E. Remiddi, Nucl. Phys. B **676** (2004) 399 [arXiv:hep-ph/0307295].
- [42] W. Bernreuther, R. Bonciani, T. Gehrmann, R. Heinesch, T. Leineweber, P. Mastrolia and E. Remiddi, Phys. Rev. Lett. **95** (2005) 261802 [arXiv:hep-ph/0509341]; Phys. Rev. D **72** (2005) 096002 [arXiv:hep-ph/0508254]; Nucl. Phys. B **712** (2005) 229 [arXiv:hep-ph/0412259]; Nucl. Phys. B **706** (2005) 245 [arXiv:hep-ph/0406046].

- [43] S. Moch, J. A. M. Vermaseren and A. Vogt, Phys. Lett. B **625** (2005) 245 [arXiv:hep-ph/0508055]; JHEP **0508** (2005) 049 [arXiv:hep-ph/0507039].
- [44] R. J. Gonsalves, Phys. Rev. Lett. **56** (1986) 1647.
- [45] R. J. Gonsalves and C. F. Wai, Phys. Rev. D **49** (1994) 190; Erratum, *ibid.* D **51** (1995) 1428. [arXiv:hep-ph/9610278].
- [46] S. Raina, “Interference phenomena in electron positron annihilation,” Ph.D. Thesis, University at Buffalo, 2002, UMI-30-52534.
- [47] R. K. Ellis, G. Martinelli and R. Petronzio, Nucl. Phys. B **211** (1983) 106.
- [48] R. J. Gonsalves, J. Pawlowski and C. F. Wai, Phys. Rev. D **40** (1989) 2245.
- [49] P. B. Arnold and M. H. Reno, Nucl. Phys. B **319** (1989) 37; Erratum, *ibid.* B **330** (1990) 284.
- [50] R. J. Gonsalves, J. Pawlowski and C. F. Wai, Phys. Lett. B **252** (1990) 663.
- [51] C. Albajar *et al.* [UA1 Collaboration], Phys. Lett. B **193** (1987) 389.
- [52] R. Ansari *et al.* [UA2 Collaboration], Phys. Lett. B **215** (1988) 175.
- [53] A. D. Martin, R. G. Roberts and W. J. Stirling, Mod. Phys. Lett. A **4** (1989) 1135.
- [54] B. Abbott *et al.* [D0 Collaboration], Phys. Lett. B **513** (2001) 292 [arXiv:hep-ex/0010026].
- [55] R. J. Gonsalves, N. Kidonakis and A. S. Vera, Phys. Rev. Lett. **95** (2005) 222001 [arXiv:hep-ph/0507317].
- [56] A. Gehrmann-De Ridder, T. Gehrmann, E. W. N. Glover and G. Heinrich, *Jet rates in electron-positron annihilation at $O(\alpha_s^3)$ in QCD*, arXiv:0802.0813 [hep-ph].
- [57] S. L. Adler, Phys. Rev. **177** (1969) 2426.
- [58] J. S. Bell and R. Jackiw, Nuovo Cim. A **60** (1969) 47.
- [59] R. K. Ellis and R. J. Gonsalves, in *Proceedings of the Oregon Workshop on Super High Energy Physics*, ed. D.E. Soper (World Scientific, Singapore, 1986), pp. 287-293.
- [60] D. A. Dicus and S. S. D. Willenbrock, Phys. Rev. D **34** (1986) 148.
- [61] R. J. Gonsalves, C. M. Hung and J. Pawlowski, Phys. Rev. D **46** (1992) 4930.
- [62] P. J. Rijken and W. L. van Neerven, Phys. Rev. D **52** (1995) 149 [arXiv:hep-ph/9501373].
- [63] A. D. Martin, R. G. Roberts, W. J. Stirling and R. S. Thorne, Eur. Phys. J. C **28** (2003) 455 [arXiv:hep-ph/0211080].